Chemistry–A European Journal
Research Article
doi.org/10.1002/chem.202200300
Chemistry Europe
European Chemical Societies Publishing
www.chemeurj.org

Cation-π Interactions between a Noble Metal and a Polyfunctional Aromatic Ligand: Ag^+(benzylamine)

Davide Corinti+,[a] Alessandro Maccelli+,[a] Barbara Chiavarino,[a] Markus Schütz,[b, c] Aude Bouchet,[b, d] Otto Dopfer,*[b] Maria Elisa Crestoni,[a] and Simonetta Fornarini*[a]

Abstract: The structure of an isolated Ag^+(benzylamine) complex is investigated by infrared multiple photon dissociation (IRMPD) spectroscopy complemented with quantum chemical calculations of candidate geometries and their vibrational spectra, aiming to ascertain the role of competing cation-N and cation-π interactions potentially offered by the polyfunctional ligand. The IRMPD spectrum has been recorded in the 800–1800 cm^{-1} fingerprint range using the IR free electron laser beamline coupled with an FT-ICR mass spectrometer at the Centre Laser Infrarouge d'Orsay (CLIO). The resulting IRMPD pattern points toward a chelate coordination (N-Ag^+-π) involving both the amino nitrogen atom and the aromatic π-system of the phenyl ring. The gas-phase reactivity of Ag^+(benzylamine) with a neutral molecular ligand (L) possessing either an amino/aza functionality or an aryl group confirms N- and π-binding affinity and suggests an augmented silver coordination in the product adduct ion Ag^+(benzylamine)(L).

Introduction

Phenylalkylamines are an important class of bifunctional compounds endowed with both a π-electron rich aromatic ring and an amino functional group representing an n-type nucleophilic site. Likely due to their potential to establish bimodal interactions, numerous phenylalkylamines are known to exert major biological functions. Catecholamines, belonging to the family of arylethylamines derived from L–DOPA, are notable examples because they have essential roles in neural transmission.[1–3] Active interest has thus grown aimed at assessing intrinsic structural features of catecholamines and phenylalkylamines in general, under unperturbed conditions as allowed by a study in the gas phase. The sampled molecules were examined as protonated species, corresponding to the prototropic form prevailing at physiological pH values. To this end, the combined approach based on infrared (IR) ion spectroscopy and quantum chemical calculations has provided detailed structural information regarding protonated molecules representative of this relevant class of compounds, including (substituted)2-phenylethylamine, ω-phenylalkylamines, and neurotransmitters such as serotonin and dopamine.[4–14]

The present work focuses on the parent phenylalkylamine, namely benzylamine ($C_6H_5CH_2NH_2$, BA). Two electron-rich functional groups of π- and n-character are separated by the methylene unit which prevents direct resonance interaction between the two sites. Any electrophile may thus select either center. For example protonation occurs exclusively at the amino group forming an ammonium ion.[8,15] As the alkyl chain joining the ammonium and phenyl ring becomes longer, the charge-bearing site may engage in cation-π interaction,[8] a binding motif that has been widely documented and characterized by IR ion spectroscopy.[16–19] Operating in an isolated state and in the absence of solvation, any effect that may contribute to charge delocalization within the charged molecule or complex tends to be magnified and exploited.

Cation-π interactions have an established important role in a variety of contexts including several fields of biology, organometallic chemistry and materials science. They typically involve an electrostatic interaction between the electron density of a π-system and a cationic site, usually a metal ion, which is also driven, even if to a lesser extent, by induction, dispersion and charge transfer.[17,20,21]

A large amount of valuable evidence is available on the competing binding of π- and n-donor sites to a metal ion in the gas phase, including metal ion interactions with substituted

[a] Dr. D. Corinti,+ Dr. A. Maccelli,+ Prof. B. Chiavarino, Prof. M. E. Crestoni, Prof. S. Fornarini
Dipartimento di Chimica e Tecnologie del Farmaco
Università degli studi di Roma La Sapienza
P.le A. Moro 5, I-00185, Roma (Italy)
E-mail: simonetta.fornarini@uniroma1.it

[b] Dr. M. Schütz, Dr. A. Bouchet, Prof. O. Dopfer
Institut für Optik und Atomare Physik
Technische Universität Berlin
Hardenbergstr. 36, 10623 Berlin (Germany)
E-mail: dopfer@physik.tu-berlin.de

[c] Dr. M. Schütz
present address: Eagleyard Photonics GmbH
Rudower Chaussee 29, 12489 Berlin (Germany)

[d] Dr. A. Bouchet
present address: Université Lille
LASIRE Lab Adv Spect Interact React & Environm
Cite Sci, CNRS, UMR 8516, 59000 Lille (France)

[+] These authors contributed equally to this manuscript.

Supporting information for this article is available on the WWW under https://doi.org/10.1002/chem.202200300

benzenes and indole[22–24] and cation-π effects in the complexation of alkali metal cations with aromatic amino acids (M^+(AAA)).[25] The latter effects are, however, estimated not to contribute significantly to the overall binding in M^+(AAA). Interactions with the amino acid backbone are rather prevailing, according to a thorough discussion based on threshold collision-induced dissociation data.[26]

In this contribution, benzylamine is let to interact with Ag^+ as selected electrophile. This cation shares similar properties with alkali metal ions. For example, its closed shell d^{10} configuration confers a prevailing electrostatic nature in ligand binding, while the tendency to form two-coordinate structures in a linear geometry has been ascribed to hybridization between the $4d_{z^2}$ and 5s orbitals resulting in sd_{z^2} hybrid orbitals.[27,28] At the same time silver is also redox active, a characteristic which is responsible for its antibacterial activity. Though not present in biological systems, Ag^+ has demonstrated an ability to bind to the aromatic portion of the side chain of amino acids and to stabilize the DNA structure.[29,30]

In a recent report, cation-π complexes of Ag^+ with benzene, toluene and furan have been studied with ultraviolet laser photodissociation and photofragment imaging, providing new information on the cation-π bond energies.[31] IR ion spectroscopy has proven to be a valuable tool to shed light on the structural features of complexes of the noble metals silver,[17,32–40] gold[41–46] and platinum,[47–53] with a variety of ligands yielding a wealth of valuable information such that only partial reference may be given here. It has been reported that complexation of Ag^+ with polycyclic aromatic hydrocarbons is accompanied by substantial charge transfer, emerging from the analysis of the IR bands of the complexes compared to those of the bare ligands.[54] In the case of phenol as ligand, the formation of an Ag^+ π-complex has been assessed by IRMPD spectroscopy, while bonding to the hydroxyl group is calculated to be less favorable.[17] In contrast, an aromatic N-heterocyclic ligand, such as pyridine (Pyr), preferably interacts with Ag^+ by the nitrogen lone pair attaining a linear Pyr–Ag^+–Pyr configuration.[55] Also in the Ag^+(uracil) complex Ag^+ binds to the n-sites, namely the N and O atoms of multiple tautomeric forms.[39] The interaction with the two diverse electron-rich groups of benzylamine needs to comply with the constraint due to the fact that the two sites are joined by a simple CH_2 linkage. The ensuing structural and reactivity features of the Ag^+(benzylamine) complex were sampled herein by IRMPD spectroscopy operated at the Centre Laser Infrarouge d'Orsay (CLIO). As usual, the experimental IRMPD spectrum was evaluated by comparison with the linear IR absorption spectra calculated for low-energy isomers. Additionally, ion-molecule reactions were investigated in the cell of an FT-ICR mass spectrometer searching for structure-specific reactivity behavior.

Experimental Section

All reagents and solvents used in this work were research grade products purchased from Sigma-Aldrich s.r.l. (Milan, Italy) and used as received. A mM methanol solution of BA and an equimolar $AgNO_3$ hydroalcoholic (CH_3OH/H_2O 1:1 v/v) solution were mixed to obtain a stock solution, which was subsequently diluted to μM range. The ions of interest Ag^+(BA) and $Ag^+(BA)_2$ were obtained by direct infusion of the μM sample solution through a fused silica capillary into an electrospray ionization (ESI) source at a flow rate of 120 $\mu L\,h^{-1}$.

MS^n experiments

Tandem MS experiments were carried out in Rome using a Paul ion trap (Esquire 3000+, Bruker Daltonics, Bremen, Germany) coupled to an ESI source working in positive polarity mode in the *m/z* 50–500 range. For each analysis, 40 scans were coadded with an accumulation time of 5 ms. In particular, peaks at *m/z* 214 and 321 (corresponding to the monoisotopic Ag^+(BA) and $Ag^+(BA)_2$ clusters, respectively) were mass isolated and fragmented by varying the resonance excitation amplitude between 0.05 and 0.70 V, to evaluate the appearance of competitive and/or consecutive fragmentation pathways.[56] Helium was used as collision gas at a nominal pressure of 1.5×10^{-6} mbar.

ESI FT-ICR MS and kinetic experiments

High-resolution mass spectra and kinetic experiments were performed in Rome using a Bruker BioApex FT-ICR mass spectrometer equipped with an Apollo I ESI source, an infinity cell and a 4.7 T superconducting magnet. Analyte solutions were directly infused in the ESI source. After desolvation by a heated (400 K) N_2 drying gas, ions were accumulated in a hexapole ion guide for 1 s to be then injected into the ICR cell kept at room temperature. Therein, ions of interest were mass isolated by ion ejection procedures and allowed to react with the selected neutral, admitted through a needle valve at a stationary pressure in the $0.4–10\times10^{-8}$ mbar range.[57] Pressure readings were measured with a cold-cathode sensor (IKR Pfeiffer Balzers S.p.A., Milan, Italy), calibrated by using the rate constant for the reference reaction $CH_4^+ + CH_4 \rightarrow CH_5^+ + CH_3^\bullet$ ($k = 1.1\times10^{-9}$ $cm^3\,s^{-1}$) and corrected for different response factors.[57] Relative abundances of the parent and product ions were monitored as a function of time.[58–60] Pseudo-first-order rate constants (*k'*) were obtained from the semilog decrease of the parent ion abundance versus time. Second-order rate constants (k_{exp}) were obtained by dividing *k'* by the neutral concentration. An estimated error in the absolute rate constants of ±30% is typically due to uncertainties in the pressure measurements. The reaction efficiencies (Φ) were obtained as the ratio between k_{exp} and the collision rate constant (k_{ADO}) calculated according to parametrized trajectory theory.[61] In addition, kinetic experiments were evaluated by using the best-fitting software GmKin (GK).[62] In this way the consecutive k_2 rate constant for a two-step reaction could be obtained.

IRMPD spectroscopy

The IRMPD spectrum of Ag^+(BA) was recorded in the fingerprint range (800–1800 cm^{-1}) using the beamline of the IR free electron laser (FEL) at CLIO. The electron energy of the FEL, operating at a repetition rate of 25 Hz, was set at 44 MeV. The FEL radiation was admitted into the cell of a hybrid FT-ICR tandem mass spectrometer (APEX-Qe Bruker) equipped with a 7.0 T actively shielded magnet and a quadrupole-hexapole interface for mass filtering and ion accumulation.[63] Ions were mass selected in the quadrupole and accumulated in the hexapole containing argon as buffer gas to permit collisional thermalization prior to their transfer into the ICR cell. Selected Ag^+(BA) ions were irradiated for 2 s with the IR FEL light, and photofragmentation was assisted by an additional CO_2

laser pulse (10 W, $\lambda = 10.6$ μm) lasting 38 ms and following a few μs after each FEL macropulse. Its chosen length ensures that no fragmentation occurred by action of the CO_2 laser only. After this sequence the resulting ions were mass-analyzed. IRMPD spectra report the photofragmentation yield R ($R = -\ln[I_{parent}/(I_{parent} + \Sigma I_{fragment})]$, where I_{parent} and $I_{fragment}$ are the integrated signals of the mass peaks of parent and fragment ions, respectively) as a function of the wavenumber of the IR radiation.

Computational details

Density functional theory (DFT) calculations were performed to optimize the geometry of the Ag^+(BA) adduct.[64] In particular, vibrational and structural features were simulated using the B3LYP functional and two different basis sets (6-311 + G(d,p) and LanL2TZ for light atoms and silver). The LanL2 pseudopotential was used for Ag core electrons, to reduce computational cost and to include relativistic effects.[65,66] Frequency analysis allowed to define whether computed stationary points could be qualified as energy minima and to obtain thermodynamic data. Calculated IR spectra are reported using a Lorentzian profile, with an associated width (FWHM) of 20 cm^{-1} for consistency with experimental spectral resolution. Mode assignment was achieved by comparison of the experimental IRMPD spectra with the calculated linear IR spectra. Harmonic vibrational frequencies were scaled by a factor of 0.96 in the sampled fingerprint range. To obtain a better simulation of non-covalent interactions, structures were re-optimized at the MP2/6-311 + G(d,p) (Ag: LanL2TZ) level.

Results and Discussion

Preparation and characterization of Ag^+(BA) adducts

The mass spectrum of a 1 : 1 solution of BA and $AgNO_3$ recorded by direct infusion-ESI on a FT-ICR instrument is reported in Figure 1. Confirmation about elemental composition of each ion was gained by both accurate mass measurements and comparison between experimental and simulated isotopic pattern. The high-mass accuracy of the FT-ICR technique has revealed Ag^+(BA) (corresponding to molecular formula C_7H_9NAg) at *m/z* 213.97792/215.97761, with a mass deviation of −0.5 ppm from the monoisotopic exact mass. The recorded isotopic distribution reported in Figure S1 in the Supporting Information clearly shows the presence of silver isotopes, ^{107}Ag and ^{109}Ag, in their natural abundance (51.84% and 48.16%), further confirming the peak assignment.

Interestingly, weak signals appear at *m/z* 321.05081/323.05067, corresponding to the $Ag^+(BA)_2$ complex. No evidence of $Ag^+(BA)_n$ complexes with $n > 2$ was detected which may be viewed as evidence for the favored Ag^+ coordination number being two.

To appraise the appearance of competitive and/or consecutive dissociation paths, both Ag^+(BA) and $Ag^+(BA)_2$ ions were submitted to collision-induced dissociation (CID) experiments. The high-resolving power of the FT-ICR analyzer has delivered accurate masses of fragments. For CID conducted on the ions with *m/z* 214, the appearance of a main fragment is revealed at *m/z* 106.06504 (Figure S2) identified as $[C_7H_8N]^+$ arising from loss of AgH. Its identity was confirmed by measuring the mass accuracy which showed an error of −0.7 ppm. This finding well matches with a previous report by Schäfer et al., showing loss of AgH as major CID process for several Ag^+(alkylamine) complexes, recognized to lead to the thermodynamically favored products.[67]

CID experiments performed in a Paul-type ion trap at varying resonance excitation amplitude has allowed to follow the appearance and development of fragmentation paths, thus resulting in the breakdown graphs reported in Figure S3, which

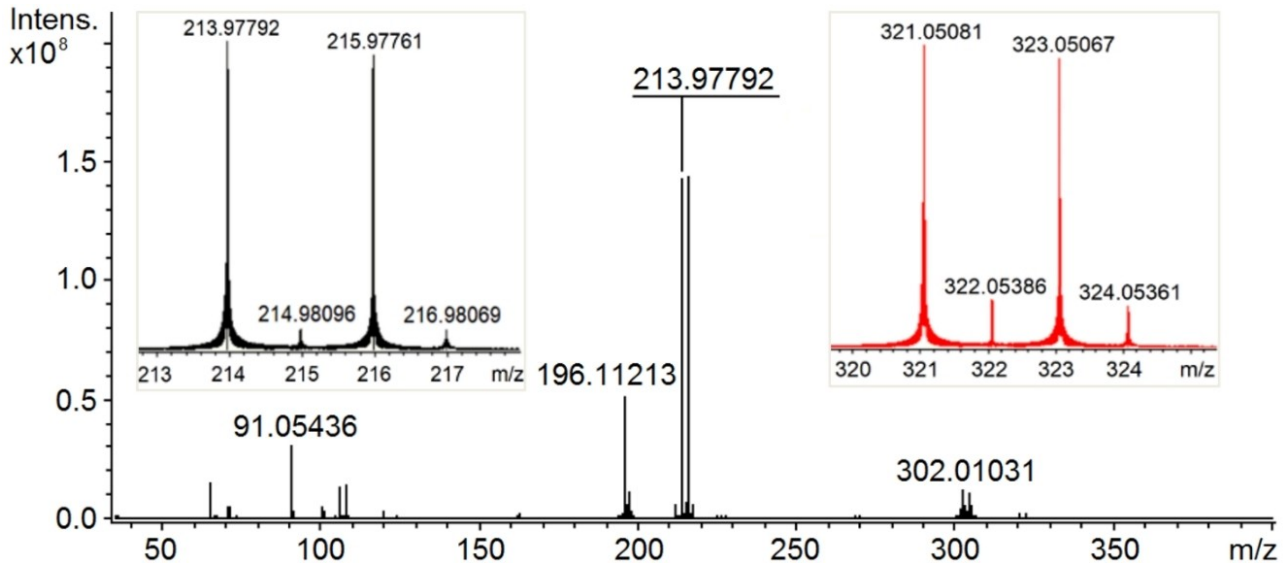

Figure 1. ESI FT-ICR mass spectrum of a of a 1 : 1 μM solution of BA and $AgNO_3$. The monoisotopic peak of the Ag^+(BA) complex (corresponding to $^{12}C_7{}^{14}NH_9{}^{107}Ag$) is detected at *m/z* 213.97792 (see Figure S1 for calculated isotopic distribution) whereas $Ag^+(BA)_2$ is revealed as tiny signals at *m/z* 321.05081/323.05067. Enlargements of signals associated to Ag^+(BA) and $Ag^+(BA)_2$ are shown in the insets (in black and red color, respectively). Ions at *m/z* 196 and 302/304 are due to the protonated ion and silver complex of a BA impurity with molecular weight of 195 u.

show relative ion abundances as a function of collisional excitation. Gas-phase dissociation of the *m/z* 214 adduct has revealed the rise of a $[C_7H_8N]^+$ (*m/z* 106) species as main fragmentation product. A minor competitive channel leads to the formation of another fragment at *m/z* 91, ascribed to $C_7H_7^+$. The dissociation of $Ag^+(BA)_2$ ions yields $Ag^+(BA)$, by loss of BA, which then undergoes the above-described dissociation paths.

IRMPD spectroscopy and structural characterization

IRMPD spectroscopy provides information about intrinsic structural features of the examined chemical species under minimal perturbation by the environment, namely in the absence of solvent and matrix effects. Furthermore, this approach permits a direct correlation between experimental results and computed geometries of candidate isomers and to assign each IRMPD band to its corresponding vibrational mode.

Irradiation with photons at 1028 cm^{-1} displays the photofragmentation products of $Ag^+(BA)$ and Figure S4 shows the mass spectrum of isolated $Ag^+(BA)$ ions recorded after irradiation. The photodissociation mass spectrum is superimposable onto the one obtained by CID (Figure S2),[56] confirming loss of AgH to be the prevailing low-energy fragmentation path.

The experimental IRMPD spectrum (red profile in Figure 2) is characterized by the presence of three dominant bands at 914,

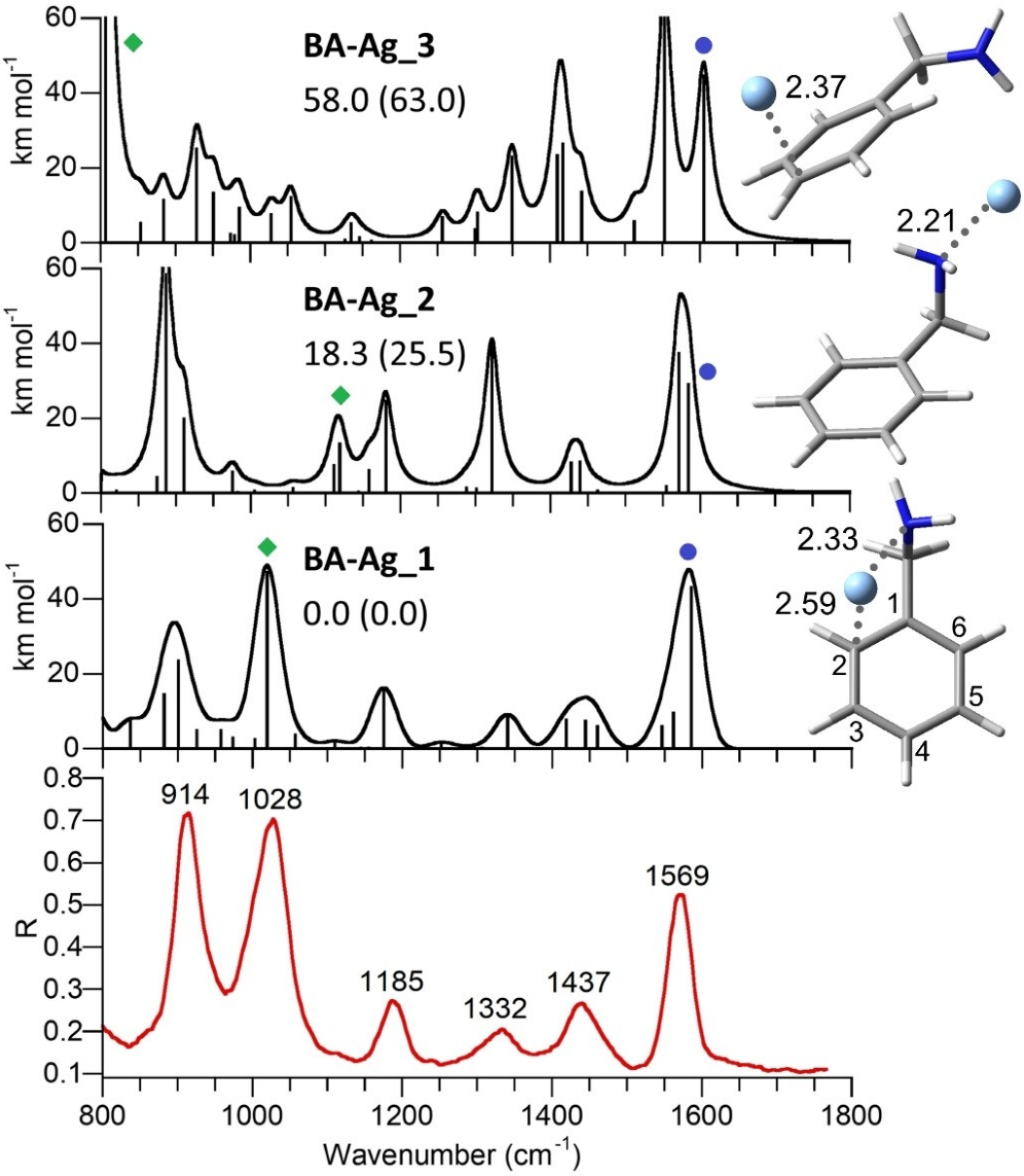

Figure 2. Calculated IR spectra (black) and experimental IRMPD spectrum (red) of mass-selected $Ag^+(BA)$ ions in the fingerprint range. Wavenumbers (in cm^{-1}) of the most important bands are reported in the IRMPD spectrum. Relevant calculated vibrational modes, NH_2 scissoring and wagging modes, are highlighted by blue circles and green diamonds, respectively. On the right side, optimized geometries of various low-energy isomers are reported. Relevant interatomic distances in Å are shown. Calculated relative free energies (298 K) at the B3LYP and MP2 (in brackets) level are reported in kJ mol^{-1}.

1028 and 1569 cm^{-1} and less pronounced features at 1185, 1332 and 1437 cm^{-1}.

The scaled harmonic IR spectra calculated for the low energy isomers BA–Ag_1, BA–Ag_2, and BA–Ag_3 were obtained for the corresponding optimized geometries (upper panels in Figure 2, Table 1). BA–Ag_1 is the most stable isomer and characterized by Ag^+ coordinated to both the amino nitrogen and the aromatic ring, with a binding energy (ΔH at 298 K) of 233 kJ mol^{-1} (at B3LYP level). Details on relevant interatomic distances are reported on the right side of Figure 2. The geometry optimized at the MP2 level shows that Ag^+ located above the aromatic plane, virtually over the C1–C2 bond in η^2 configuration, with bond lengths of 2.78 and 2.59 Å for Ag–C1 and Ag–C2, respectively. This coordination mode, where the metal ion resides above the midpoint of a C–C bond near the edge of an aromatic ring, is a common structural feature in Ag^+(arene) complexes.[31,54] In this conformation, the C2–H2 bond appears to be tilted out of the aromatic plane by an angle of 8.5° in the opposite direction relative to the metal ion. Moreover, Ag^+ is bound to the amino nitrogen, located at a distance of 2.33 Å. The higher-energy isomers BA–Ag_2 and BA–Ag_3 display a single coordination motif for Ag^+, bound to either the amino nitrogen or the aromatic ring, respectively. The interaction with nitrogen is thermodynamically favored. In fact, the relative free energy of BA–Ag_2 is 25.5 kJ mol^{-1} (MP2), much lower than the one of BA–Ag_3 (63.0 kJ mol^{-1}). The charge distribution in BA–Ag_1-3, as obtained by natural population analysis, is reported in Figure S5. The positive charge remains largely localized on silver, in agreement with relative ionization energies of 7.58 and 8.5 eV for Ag and BA, respectively.[68] One may note that the positive charge on silver is lowest (0.918) in BA–Ag_1, consistent with the cooperative π- and N-interaction.

By comparing the IRMPD profile with the calculated IR spectra, a very good match with the most stable isomer BA–Ag_1 is clear, thus confirming the metal chelate coordination (N–Ag^+–π) with both the amino nitrogen and the aromatic ring as the prevailing binding motif in the sampled ions. Comparing the three calculated harmonic spectra highlights the presence of mainly two vibrational modes that are influenced by the different Ag^+ binding sites, namely the NH_2 scissoring and NH_2 wagging modes. The former is computed near 1585 cm^{-1} for both BA–Ag_1 and BA–Ag_2. However, BA–Ag_3, which lacks the N-Ag^+ interaction, displays a slightly higher frequency for this mode (1605 cm^{-1}), thus modifying the profile of the calculated spectrum in this spectral range. The effect of Ag^+ coordination on the NH_2 wagging is more pronounced and goes in parallel with the magnitude of the Ag^+-N interaction. In particular, a linear correlation is found between the partial negative charge on N and the wagging frequency. In BA–Ag_2, where Ag^+ is bound only to the amino nitrogen, the NH_2 wagging mode is observed at the relatively high frequency of 1119 cm^{-1}. In contrast, the same mode in BA–Ag_3, which has a free NH_2 group, is calculated at 807 cm^{-1}. Coherently, BA–Ag_1 presents an intermediate situation, with the NH_2 wagging located at 1020 cm^{-1}. Indeed, a strong IRMPD band is observed at 1028 cm^{-1}. In consideration of the nearly background activity observed in the IRMPD spectrum at the wagging frequencies of BA–Ag_2 and BA–Ag_3, one may estimate the contribution of these isomers to be less than 10% in the sampled ion population.

Table 1 lists wavenumbers and relative intensities (in parentheses) of the main IRMPD absorptions. The vibrational mode assignment is also reported, as derived from the calculated IR spectrum of BA–Ag_1. As already evident from the very good matching between the experimental spectrum and the computed IR spectrum of BA–Ag_1 displayed in Figure 2, one finds satisfactory agreement between experimental and calculated frequencies. The largest deviation amounts to 16 cm^{-1}, with an average deviation of 10 cm^{-1}, confirming the vibrational and isomer assignments given in Table 1. Interestingly, even modes with calculated oscillator strengths somewhat below 10 km mol^{-1} are well observed in the IRMPD spectrum. A complete list of vibrational modes pertaining to all three BA–Ag_1-3 isomers is provided in Table S1.

Table 1. Observed IRMPD bands of the Ag^+(BA) complex and calculated vibrational frequencies of BA–Ag_1.

Wavenumber [cm^{-1}] IRMPD	Calculated[a] BA–Ag_1	Assigned vibrational mode[b]
914	882 (15)	rock CH_2–σ C–N–β NH
	901 (24)	β oop H_{ar} – β oop C_{ar}
1028	1020 (47)	wag NH_2
1185	1175 (16)	σ C_{ar}–C_{benz}
1332	1341 (9)	wag CH_2–twist NH_2
1437	1419 (8)	β ip CH_{ar}–σCC_{ar}
	1444 (7)	sciss CH_2
	1460 (6)	β ip CH_{ar}
1569	1547 (6)	ring breathing
	1562 (10)	ring breathing
	1585 (43)	sciss NH_2

[a] Vibrational modes obtained at the B3LYP/6-311 + G(d,p) level (Ag = LanL2TZ). Intensities in km mol^{-1} in parentheses. [b] β = bending; σ = stretching; rock = rocking; wag = wagging; sciss = scissoring; twist = twisting; ip = in plane; oop = out of plane; ar = aromatic; benz = benzylic.

Ion-molecule reactions

The reactivity of $Ag^+(BA)$ ions toward a few neutral ligands (L) possessing an N atom and/or an aromatic ring has been investigated by ESI FT-ICR mass spectrometry. The sampled ions, obtained in solution and transferred into the gas phase by the ESI process, were guided into the ICR cell to test their reactivity with L and eventually to obtain some insight related to their structure. It may be expected that separating the functional groups (phenyl and amino moieties) present in BA into distinct molecular reagents (such as an aromatic hydrocarbon and an amine) would produce poorly efficient ligands in replacing BA and substitution reactions should hardly be observed. Coordination at the metal would in fact be depleted by an entering monofunctional ligand if the $Ag^+(BA)$ complex were stabilized by chelate BA binding. When $Ag^+(BA)$ ions were let to react with a stationary concentration of L (L = toluene, mesitylene, pyridine, and piperidine, henceforth abbreviated as Tol, Mes, Pyr, Pip, respectively), a primary addition product was observed with all examined ligands. In no case was a ligand substitution product observed. All reactions led to the complete disappearance of the reactant ion, according to Equation (1). Only in the case of the reaction with Pip, a further step involving BA substitution occurs after the first addition, as outlined in Equation (2).

$$Ag^+(BA) + L \rightarrow Ag^+(BA)(L) \quad (1)$$

$$Ag^+(BA)(L) + L \rightarrow Ag^+(L)_2 + BA \quad (2)$$

The time dependence of ion abundances is exemplified by the reaction with Tol and Pip, conforming to addition and addition + substitution, respectively (Figure 3). The fitted kinetic curves (dashed lines) well match the experimental data.

The formation of the $Ag^+(BA)(L)$ adduct with L = Mes ion is shown in the ESI FT-ICR mass spectrum reported in Figure S6, while the formation of both $Ag^+(BA)(L)$ and $Ag^+(L)_2$ ions with L = Pip is displayed in the mass spectrum shown in Figure S7. Representative plots of ion abundancies as a function of time are reported in Figure S8 for L = Mes and Pyr. Second-order rate constants (k_{exp}) along with reaction efficiencies (Φ) are reported in Table 2.

The kinetic efficiency values show Tol to be the least reactive among the tested ligands. A fairly activated arene such as Mes is three times more efficient. A somewhat surprising result concerns Pyr and Pip showing comparable efficiency as the aromatic hydrocarbons. Also listed in Table 2 are the proton affinity (PA) values of each ligand. This thermodynamic parameter is defined as $-\Delta H$ for the attachment of a proton to the isolated molecule in the gas phase. The proton affinity is obviously not an ideal parameter for comprehending the

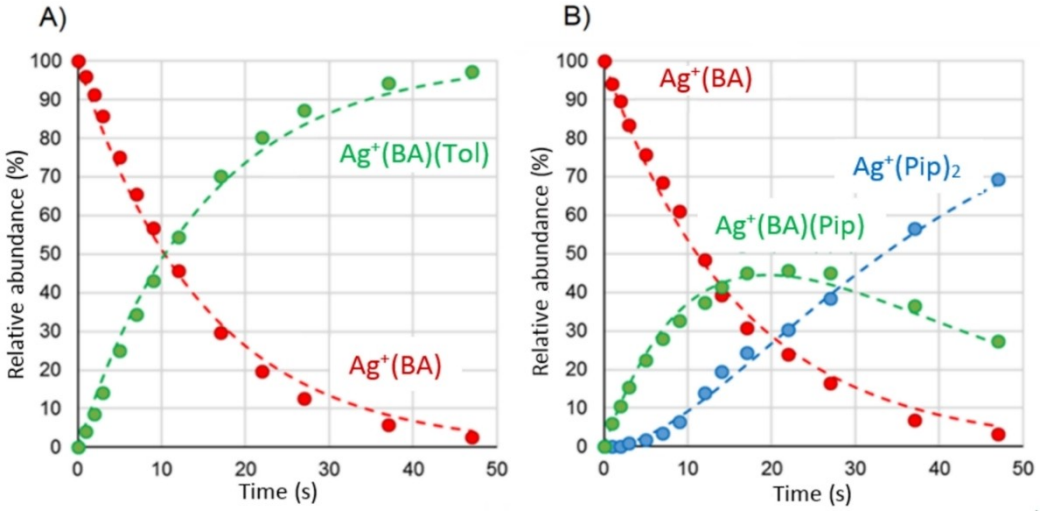

Figure 3. Time dependence of ion abundances for the $Ag^+(BA)$ reaction with toluene (panel A) at 2.5×10^{-8} mbar and piperidine at 4.5×10^{-9} mbar (panel B). Dashed lines represent fitted kinetic curves.

Table 2. Kinetic data for the gas phase reaction of $Ag^+(BA)$ ions with selected neutrals (L).

L	Proton affinity [kJ mol^{-1}][68]	k_{exp} [10^{-10} cm^3 molecule^{-1} s^{-1}]	Φ[a]
Toluene	784	1.2	12
Mesitylene	836	3.4	31
Pyridine	930	3.7	24
Piperidine[b]	954	5.8	47

[a] Reaction efficiency: $\Phi = (k_{exp}/k_{coll})\times100$. [b] A rate constant $k_2 = 0.34\times10^{-10}$ cm^3 molecule^{-1} s^{-1} is obtaned for the ligand displacement [Equation (2)].[62]

behavior of the Ag^+ ion, which is much softer than the proton.[69,70] A sodium affinity scale could provide more proper values for evaluation of the results. However, sodium affinities are not available for all ligands, nor are other alkali metal ion affinity values. It is found, though, that alkali metal ion binding energies follow the same trends as PAs.[25] This notion is in fact verified by the sodium affinity for toluene (113 kJ mol^{-1})[23] and for pyridine (127 kJ mol^{-1})[71] to be compared with PA values of 784 and 930 kJ mol^{-1}, respectively.[68] A 12–18% increase in sodium/proton affinity is observed for pyridine compared with toluene. Thus, the listed PA values may assist in some reasoning. To start with, it is noteworthy that a powerful base such as Pip, which can only provide coordination via the N atom, does not displace the less basic BA (PA = 913 kJ mol^{-1}). This negative evidence suggests that ligand exchange may be energetically unfavorable and supports the chelate coordination of BA through both n- and π-donation. Ligand displacement occurs only as a second step and the ultimate formation of $Ag^+(L)_2$ with L = Pip may reflect the presence of only this neutral in the FT-ICR cell, driving the reaction irreversibly. The rate constant for this consecutive step corresponding to an efficiency of only 3.0% may be viewed as another effect of the powerful coordination exerted by BA, making it a reluctant leaving group. As noted above, no displacement reaction is observed for the other tested ligands.

While the electron-deficient π-ring of pyridine is not prone to engage in Ag^+ binding,[55] the reaction efficiencies of pure π-ligands in the addition reaction appear remarkable. Mes is nearly as efficient as Pip in forming Ag^+(BA)(L), indicative of the notable affinity of Ag^+ for coordination to π-systems. On the other hand, the significant affinity of Ag^+ toward π-donors relative to N-donors is already testified by the Ag^+-L binding energy (BE) when L is the parent aromatic ring or parent amine, namely benzene and ammonia. In spite of a large PA difference favoring NH_3 by > 100 kJ mol^{-1},[68] the BE values are approximately the same for L = C_6H_6 and NH_3 (ca. 159[16,71,72] and 170 kJ mol^{-1},[71–73] respectively).

Geometry of gas-phase Ag^+(BA)(L) adduct ions

Additional insight into the structure of so-formed Ag^+(BA)(L) ions has been sought by quantum chemical computations. To evaluate plausible isomeric structures for the adduct ions obtained by the reaction of Ag^+(BA) with selected ligands, a computational survey has been performed. Concerning the structure of Ag^+(BA)(L), three sets of geometries were considered, formally derived from the three distinct structures of Ag^+(BA) reported in Figure 2 by association of the second ligand. The optimized geometries thus obtained are displayed in Figure 4. In all structures listed in the first column, the Ag^+(BA) unit retains the chelate coordination geometry that was found to be the most stable one (BA–Ag_1), prevailing in the sampled population. In the second column, the Ag^+(BA) unit is ligated by N-coordination to the metal (as in BA–Ag_2), while in the third column Ag^+(BA) is bound by π-coordination (as in BA–Ag_3). Each Ag^+(BA) moiety is then allowed to interact with L and the resulting adducts were optimized at both B3LYP/6-311 + G(d,p) and MP2/6-311 + G(d,p) levels of theory. While Figure 4 collects structures from MP2/6-311 + G(d,p) optimizations, the results of computations at the B3LYP/6-311 + G(d,p) level are shown in Figure S9.

Table 3 shows the thermodynamic data for the computed structures according to the two levels of theory employed. In all cases, B3LYP results indicate isomers of series 1 and 2 to be very close both in relative enthalpy and in relative free energy. In contrast, the folded structures of series 1 are favored by ≥ 8 kJ mol^{-1} in relative G according to MP2 data. This finding can be related to B3LYP not being able to properly simulate the non-covalent interaction of Ag^+ with the aromatic ring.[74,75] Elements of series 3 are consistently higher in enthalpy (free energy) by ≥ 49 (44) kJ mol^{-1} according to either computational approach.

A few geometrical features related to the Ag^+(BA)(L) complexes with L = Mes (representative π-ligand) and L = Pip (representative N-ligand) may deserve a comment. In general,

Table 3. Computed thermodynamic data for Ag^+(BA)(L) isomers together with ligand binding energies (BEs).

Isomers	B3LYP[a]				MP2[a]			
	H_{rel}[b]	G_{rel}[b]	BE[c] H[b]	G[b]	H_{rel}[b]	G_{rel}[b]	BE[c] H[b]	G[b]
BA_Ag_1_Tol	0.0	0.0	103.5	59.6	0.0	0.0	119.2	79.6
BA_Ag_2_Tol	6.6	0.5			26.1	17.6		
BA_Ag_3_Tol	56.6	47.5			53.5	53.1		
BA_Ag_1_Mes	0.0	0.0	108.3	70.3	0.0	0.0	140.7	88.3
BA_Ag_2_Mes	1.2	−0.9			28.4	11.1		
BA_Ag_3_Mes	51.5	45.4			49.5	44.5		
BA_Ag_1_Pyr	0.0	0.00	159.4	119.3	0.0	0.0	157.8	115.4
BA_Ag_2_Pyr	0.6	−0.18			16.2	9.2		
BA_Ag_3_Pyr	54.9	50.0			53.9	45.7		
BA_Ag_1_Pip	0.0	0.0	161.6	120.6	0.0	0.0	166.5	121.5
BA_Ag_2_Pip	−0.3	0.03			18.0	8.3		
BA_Ag_3_Pip	54.0	50.3			51.3	58.9		

[a] 6-311 + G(d,p) and LanL2TZ for light atoms and silver, respectively, [b] 298 K, in kJ mol^{-1}. [c] BEs report $-\Delta H/\Delta G$ for the process: Ag^+(BA) + L → Ag^+(BA)(L), L = Tol, Mes, Pyr, Pip.

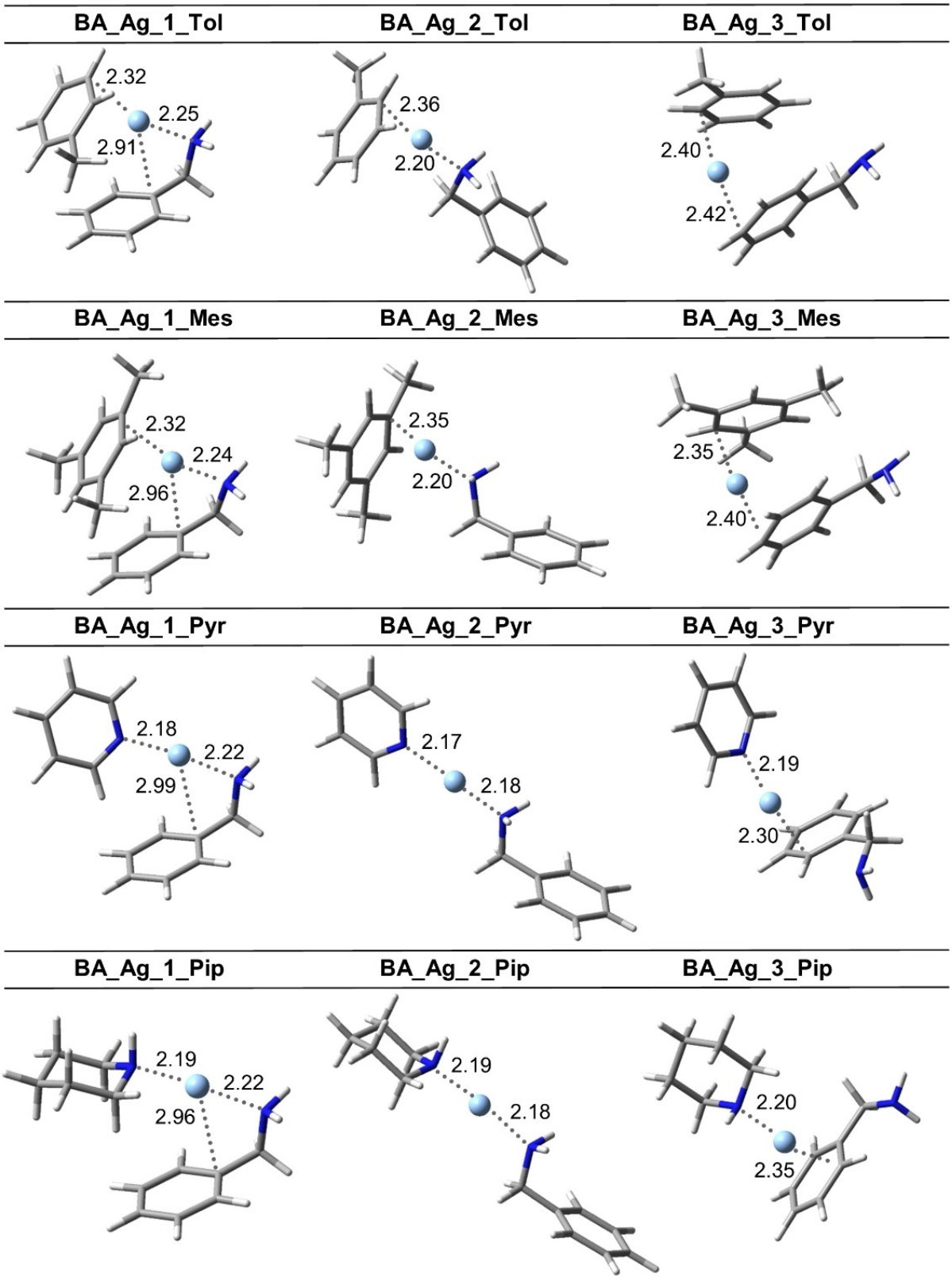

Figure 4. Optimized geometries for Ag^{+}(BA)(L) ions (L = Tol, Mes, Pyr, Pip) at the MP2 level. Bond distances (in Å) are indicated by dashed lines.

the folded structures of series 1 complexes maintain the binding motifs already present in BA_Ag_1. Comparatively, the presence of Mes as additional ligand in BA_Ag_1_Mes strengthens the Ag^{+}-N interaction (bond length varies from 2.33 to

2.24 Å in BA_Ag_1 and BA_Ag_1_Mes, respectively), while weakening the Ag^+-π interaction (Ag–C1 bond length varies from 2.78 to 2.96 Å in BA_Ag_1 and BA_Ag_1_Mes, respectively). The electron-rich character of the Mes ring is reflected in the rather short Ag–CH(Mes) distance of 2.32 Å, to be compared with the lengthened Ag–C1(BA) distance of 2.96 Å. The latter value is also found for BA_Ag_1_Pip, in which the two N(Pip) and N(BA) atoms share an approximately linear Ag ligation at 2.19 and 2.22 Å distance, respectively. It is worthwhile to underline here that the drive towards attaining a linear coordination geometry has been recently reported also for the hydrated Ag^+ ion in aqueous solution, as indicated by results combining X-ray absorption spectroscopy with ab initio MD simulations.[27] The preference for a first shell linear coordination that is well ascertained for $[Ag(H_2O)_2]^+$ in the solid state is thus found to emerge also in the more complex solution environment. The tendency of the metal to attain the favored linear coordination is ubiquitous in the structures displayed in Figure 4. It appears also in BA_Ag_3_Mes, for which the Ag–CH(Mes) and Ag–C4(BA) distances of 2.35 and 2.40 Å reflect the stronger activation of the mesitylene π-system. As already observed for BA_Ag_1_Mes, the increased silver coordination in BA_Ag_1_Pip moves the BA ring carbon to 2.96 Å from the original distance of 2.78 Å in BA_Ag_1, likely due to steric hindrance in attaining a proper arrangement of the increased ligation sites around the metal.

Association free energy and reactivity

Generally, gas-phase association reactions conducted below the high-pressure limit are considered barrierless,[76–78] so that a correlation is expected between the binding free energy of $Ag^+(BA)(L)$ complexes and the kinetics of the corresponding $Ag^+(BA) + L$ association process.[76–78] Binding energies were then calculated at both adopted levels of theory by relating each addition complex to the reference state represented by the most stable Ag^+(BA) structure (BA–Ag_1) and the selected neutral ligand as separated partners. Results are reported in Table 3, showing N-ligands to be favored for both enthalpy and free energy reasons. Differences become smaller when viewing the results at the MP2 level. For example, the difference in association free energy between Mes and Pyr amounts to 49.0 kJ mol^{-1} according to B3LYP data and to 27.1 kJ mol^{-1} from MP2 calculations. Clearly the latter approach is better suited to describe delocalized non-covalent interactions engaging a π-electron system. The soft BA-ligated Ag^+ shows remarkable affinity for the arene ligands. This notion may be evidenced by the span in proton affinity between Pip and Tol of 170 kJ mol^{-1} (Table 2), which reduces to 47.3 kJ mol^{-1} when the MP2 binding enthalpy of the two ligands to Ag^+(BA) is considered. Thus, though failing to account for the somewhat higher association efficiency of Mes relative to Pyr, the computational results confirm the noteworthy tendency of Ag^+ to establish highly favored, if not preferential, cation-π relative to cation-N interactions. Within the same coordination mode, the binding energy data quite confirm the Mes > Tol and Pip > Pyr efficiency trend.

Conclusion

Ag^+(BA) ions represent a simple prototypical model system, in which Ag^+ is allowed to interact with π-type and/or N-donor sites that are separated by a methylene bridge. The most stable geometry, namely BA–Ag_1, is found to display a folded N–Ag^+–π chelate conformation allowing both Ag^+–π and Ag^+–N interactions. This structure is clearly evidenced by the IRMPD spectrum recorded on the naked ion delivered by ESI from solution into the gas phase. Alternative geometries enabling just either Ag^+–π or Ag^+–N coordination lie at 26 and 63 kJ mol^{-1} in relative free energy (MP2), and no significant contribution is ascribable to these species in the sampled ion population. The remarkable affinity of Ag^+ for π-donors is well evidenced by the kinetic study of the ligand addition reaction $Ag^+(BA) + L \rightarrow Ag^+(BA)(L)$. Reaction efficiencies for the association of Ag^+(BA) with L = toluene, mesitylene, pyridine, and piperidine lie all within the same order of magnitude, in spite of widely different proton affinities of L ranging from 784 kJ mol^{-1} (Tol) to 954 kJ mol^{-1} (Pip). The rather narrow range in the reaction efficiency trend, toluene < pyridine < mesitylene < piperidine, is instead fairly in line with Ag^+(BA) association enthalpy values, covering a rather small 47 kJ mol^{-1} gap. The major issue here is that the affinity of π-ligands is quite comparable to that of N-ligands. The reported computed data for Ag^+(BA) ligand addition refer to the thermodynamically favored process starting from BA–Ag_1 and leading to a $Ag^+(BA)(L)$ adduct in which the bidentate BA coordination to Ag^+ is maintained. It may be underlined that the increased coordination around the metal in forming the BA_Ag_1_L family of complexes yields rather folded structures, quite different from the more expanded and flexible BA_Ag_2_L and BA_Ag_3_L series for which BA ligation is limited to the N- or π-site, respectively. Forthcoming studies are planned to gain experimental evidence about the structure of Ag^+(BA)(L) complexes, based on IRMPD spectroscopy and ion mobility mass spectrometry.[79–81]

Acknowledgements

This work was financially supported by the Italian Ministry for Education, University and Research – Dipartimenti di Eccellenza – L. 232/2016, the Deutsche Forschungsgemeinschaft (DO 729/3) and the EU Union's Horizon 2020 research and innovation programme under grant agreement No 731077 (EU_FT-ICR_MS) and grant agreement No. 730872 (CALIPSOPlus). We are grateful to Jean-Michel Ortega and Estelle Loire and to the CLIO team for helpful assistance. Open Access Funding provided by Universita degli Studi di Roma La Sapienza within the CRUI-CARE Agreement.

Conflict of Interest

The authors declare no conflict of interest.

Data Availability Statement

The data that support the findings of this study are available in the supplementary material of this article.

Keywords: ion-molecule reactions · IRMPD spectroscopy · mass spectrometry · non-covalent interactions · structure elucidation

[1] R. Kvetnansky, E. L. Sabban, M. Palkovits, *Physiol. Rev.* **2009**, *89*, 535–606.
[2] J. Prince, *J. Clin. Psychopharmacol.* **2008**, *28*, S39-S45.
[3] H. Reis, C. Guatimosim, M. Paquet, M. Santos, F. Ribeiro, A. Kummer, G. Schenatto, J. Salgado, L. Vieira, A. Teixeira, A. Palotas, *Curr. Med. Chem.* **2009**, *16*, 796–840.
[4] A. Bouchet, M. Schütz, B. Chiavarino, M. E. Crestoni, S. Fornarini, O. Dopfer, *Phys. Chem. Chem. Phys.* **2015**, *17*, 25742–25754.
[5] A. Bouchet, M. Schütz, O. Dopfer, *ChemPhysChem* **2016**, *17*, 232–243.
[6] M. Schütz, A. Bouchet, B. Chiavarino, M. E. Crestoni, S. Fornarini, O. Dopfer, *Chem. Eur. J.* **2016**, *22*, 8124–8136.
[7] M. Schütz, A. Bouchet, O. Dopfer, *Phys. Chem. Chem. Phys.* **2016**, *18*, 26980–26989.
[8] B. Chiavarino, M. E. Crestoni, M. Schütz, A. Bouchet, S. Piccirillo, V. Steinmetz, O. Dopfer, S. Fornarini, *J. Phys. Chem. A* **2014**, *118*, 7130–7138.
[9] A. Lagutschenkov, J. Langer, G. Berden, J. Oomens, O. Dopfer, *Phys. Chem. Chem. Phys.* **2011**, *13*, 2815–2823.
[10] A. Lagutschenkov, J. Langer, G. Berden, J. Oomens, O. Dopfer, *J. Phys. Chem. A* **2010**, *114*, 13268–13276.
[11] A. Lagutschenkov, J. Langer, G. Berden, J. Oomens, O. Dopfer, *Phys. Chem. Chem. Phys.* **2011**, *13*, 15644.
[12] T. D. Vaden, T. S. J. A. de Boer, N. A. MacLeod, E. M. Marzluff, J. P. Simons, L. C. Snoek, *Phys. Chem. Chem. Phys.* **2007**, *9*, 2549.
[13] N. A. Macleod, J. P. Simons, *Mol. Phys.* **2007**, *105*, 689–700.
[14] G. Féraud, M. Broquier, C. Dedonder-Lardeux, G. Grégoire, S. Soorkia, C. Jouvet, *Phys. Chem. Chem. Phys.* **2014**, *16*, 5250.
[15] G. Bouchoux, J.-Y. Salpin, *Mass Spectrom. Rev.* **2012**, *31*, 353–390.
[16] M. A. Duncan, *Int. J. Mass Spectrom.* **2008**, *272*, 99–118.
[17] A. Lagutschenkov, R. K. Sinha, P. Maitre, O. Dopfer, *J. Phys. Chem. A* **2010**, *114*, 11053–11059.
[18] D. T. Moore, J. Oomens, J. R. Eyler, G. von Helden, G. Meijer, R. C. Dunbar, *J. Am. Chem. Soc.* **2005**, *127*, 7243–7254.
[19] R. C. Dunbar, J. D. Steill, J. Oomens, *J. Am. Chem. Soc.* **2011**, *133*, 1212–1215.
[20] A. S. Mahadevi, G. N. Sastry, *Chem. Rev.* **2013**, *113*, 2100–2138.
[21] J. C. Ma, D. A. Dougherty, *Chem. Rev.* **1997**, *97*, 1303–1324.
[22] V. Ryzhov, R. C. Dunbar, *J. Am. Chem. Soc.* **1999**, *121*, 2259–2268.
[23] R. Amunugama, M. T. Rodgers, *J. Phys. Chem. A* **2002**, *106*, 5529–5539.
[24] R. Amunugama, M. T. Rodgers, *Int. J. Mass Spectrom.* **2003**, *222*, 431–450.
[25] V. Ryzhov, R. C. Dunbar, B. Cerda, C. Wesdemiotis, *J. Am. Soc. Mass Spectrom.* **2000**, *11*, 1037–1046.
[26] C. Ruan, M. T. Rodgers, *J. Am. Chem. Soc.* **2004**, *126*, 14600–14610.
[27] M. Busato, A. Melchior, V. Migliorati, A. Colella, I. Persson, G. Mancini, D. Veclani, P. D'Angelo, *Inorg. Chem.* **2020**, *59*, 17291–17302.
[28] L. E. Orgel, *J. Chem. Soc.* **1958**, 4186–4190.
[29] N. C. Polfer, J. Oomens, R. C. Dunbar, *Phys. Chem. Chem. Phys.* **2006**, *8*, 2744.
[30] S. Johannsen, N. Megger, D. Böhme, R. K. O. Sigel, J. Müller, *Nat. Chem.* **2010**, *2*, 229–234.
[31] B. M. Rittgers, D. Leicht, M. A. Duncan, *J. Phys. Chem. A* **2020**, *124*, 9166–9176.
[32] A. D. Brathwaite, T. B. Ward, J. H. Marks, M. A. Duncan, *J. Phys. Chem. A* **2020**, *124*, 8562–8573.
[33] N. C. Polfer, J. Oomens, D. T. Moore, G. von Helden, G. Meijer, R. C. Dunbar, *J. Am. Chem. Soc.* **2006**, *128*, 517–525.
[34] M. W. Forbes, M. F. Bush, N. C. Polfer, J. Oomens, R. C. Dunbar, E. R. Williams, R. A. Jockusch, *J. Phys. Chem. A* **2007**, *111*, 11759–11770.
[35] T. Iino, K. Ohashi, K. Inoue, K. Judai, N. Nishi, H. Sekiya, *Eur. Phys. J. D* **2007**, *43*, 37–40.
[36] K. Inoue, K. Ohashi, T. Iino, J. Sasaki, K. Judai, N. Nishi, H. Sekiya, *Phys. Chem. Chem. Phys.* **2008**, *10*, 3052.
[37] A. Günther, P. Nieto, G. Berden, J. Oomens, O. Dopfer, *Phys. Chem. Chem. Phys.* **2014**, *16*, 14161–14171.
[38] P. Nieto, A. Günther, G. Berden, J. Oomens, O. Dopfer, *J. Phys. Chem. A* **2016**, *120*, 8297–8308.
[39] T. E. Akinyemi, R. R. Wu, Y.-W. Nei, N. A. Cunningham, H. A. Roy, J. D. Steill, G. Berden, J. Oomens, M. T. Rodgers, *J. Am. Soc. Mass Spectrom.* **2017**, *28*, 2438–2453.
[40] G. Niedner-Schatteburg, M. M. Kappes, *Chem. Eur. J.* **2021**, *27*, 15028–15043.
[41] J. Schulz, L. Jašíková, A. Škríba, J. Roithová, *J. Am. Chem. Soc.* **2014**, *136*, 11513–11523.
[42] J. Schulz, J. Jašík, A. Gray, J. Roithová, *Chem. Eur. J.* **2016**, *22*, 9827–9834.
[43] P. Motloch, J. Jašík, J. Roithová, *Organometallics* **2021**, *40*, 1492–1502.
[44] J. Roithová, J. M. Bakker, *Mass Spectrom. Rev.* **2021**, mas.21698.
[45] P. B. Armentrout, B. C. Stevenson, F. Yang, F. J. Wensink, O. V. Lushchikova, J. M. Bakker, *J. Phys. Chem. A* **2019**, *123*, 8932–8941.
[46] S. M. Lang, T. M. Bernhardt, J. M. Bakker, B. Yoon, U. Landman, *J. Am. Soc. Mass Spectrom.* **2019**, *30*, 1895–1905.
[47] O. W. Wheeler, M. Salem, A. Gao, J. M. Bakker, P. B. Armentrout, *J. Phys. Chem. A* **2016**, *120*, 6216–6227.
[48] D. Corinti, G. Frison, B. Chiavarino, E. Gabano, D. Osella, M. E. Crestoni, S. Fornarini, *Angew. Chem. Int. Ed.* **2020**, *59*, 15595–15598; *Angew. Chem.* **2020**, *132*, 15725–15728.
[49] D. Corinti, M. E. Crestoni, S. Fornarini, E. Dabbish, E. Sicilia, E. Gabano, E. Perin, D. Osella, *J. Biol. Inorg. Chem.* **2020**, *25*, 655–670.
[50] D. Corinti, M. E. Crestoni, B. Chiavarino, S. Fornarini, D. Scuderi, J.-Y. Salpin, *J. Am. Soc. Mass Spectrom.* **2020**, *31*, 946–960.
[51] D. Corinti, M. E. Crestoni, S. Fornarini, F. Ponte, N. Russo, E. Sicilia, E. Gabano, D. Osella, *J. Am. Soc. Mass Spectrom.* **2019**, *30*, 1881–1894.
[52] D. Corinti, C. Coletti, N. Re, R. Paciotti, P. Maître, B. Chiavarino, M. E. Crestoni, S. Fornarini, *Int. J. Mass Spectrom.* **2019**, *435*, 7–17.
[53] C. C. He, L. A. Hamlow, B. Kimutai, H. A. Roy, Z. J. Devereaux, N. A. Cunningham, J. Martens, G. Berden, J. Oomens, C. S. Chow, M. T. Rodgers, *Phys. Chem. Chem. Phys.* **2021**, *23*, 21959–21971.
[54] M. Savoca, T. Wende, L. Jiang, J. Langer, G. Meijer, O. Dopfer, K. R. Asmis, *J. Phys. Chem. Lett.* **2011**, *2*, 2052–2056.
[55] S. Chakraborty, O. Dopfer, *ChemPhysChem* **2011**, *12*, 1999–2008.
[56] F. Falvo, L. Fiebig, F. Dreiocker, R. Wang, P. B. Armentrout, M. Schäfer, *Int. J. Mass Spectrom.* **2012**, *330–332*, 124–133.
[57] D. Corinti, M. E. Crestoni, S. Fornarini, M. Pieper, K. Niehaus, M. Giampà, *Anal. Bioanal. Chem.* **2019**, *411*, 953–964.
[58] S. Gronert, *Mass Spectrom. Rev.* **2005**, 24, 100–120.
[59] T. Waters, R. A. J. O'Hair, A. G. Wedd, *J. Am. Chem. Soc.* **2003**, *125*, 3384–3396.
[60] D. G. Harman, S. J. Blanksby, *Org. Biomol. Chem.* **2007**, *5*, 3495–3503.
[61] T. Su, W. J. Chesnavich, *J. Chem. Phys.* **1982**, *76*, 5183–5185.
[62] https://cran.r-project.org/web/packages/mkin/index.html Version 0.9.50.2 Accessed 01 Sept. **2020**.
[63] J. M. Bakker, T. Besson, J. Lemaire, D. Scuderi, P. Maître, *J. Phys. Chem. A* **2007**, *111*, 13415–13424.
[64] M. J. Frisch, G. W. Trucks, H. B. Schlegel, G. E. Scuseria, M. A. Robb, J. R. Cheeseman, G. Scalmani, V. Barone, B. Mennucci, G. A. Petersson, H. Nakatsuji, M. Caricato, X. Li, H. P. Hratchian, A. F. Izmaylov, J. Bloino, G. Zheng, J. L. Sonnenberg, M. Hada, M. Ehara, K. Toyota, R. Fukuda, J. Hasegawa, M. Ishida, T. Nakajima, Y. Honda, O. Kitao, H. Nakai, T. Vreven, J. A. Montgomery, Jr., J. E. Peralta, F. Ogliaro, M. Bearpark, J. J. Heyd, E. Brothers, K. N. Kudin, V. N. Staroverov, R. Kobayashi, J. Normand, K. Raghavachari, A. Rendell, J. C. Burant, S. S. Iyengar, J. Tomasi, M. Cossi, N. Rega, J. M. Millam, M. Klene, J. E. Knox, J. B. Cross, V. Bakken, C. Adamo, J. Jaramillo, R. Gomperts, R. E. Stratmann, O. Yazyev, A. J. Austin, R. Cammi, C. Pomelli, J. W. Ochterski, R. L. Martin, K. Morokuma, V. G. Zakrzewski, G. A. Voth, P. Salvador, J. J. Dannenberg, S. Dapprich, A. D. Daniels, Ö. Farkas, J. B. Foresman, J. V. Ortiz, J. Cioslowski, and D. J. Fox, Gaussian, Inc., Wallingford CT, **2009**. Gaussian09, Revision D.01.
[65] P. J. Hay, W. R. Wadt, *J. Chem. Phys.* **1985**, *82*, 270–283.
[66] H. Schwarz, *Angew. Chem. Int. Ed.* **2003**, *42*, 4442–4454; *Angew. Chem.* **2003**, *115*, 4580–4593.
[67] M. Schäfer, F. Dreiocker, H. Budzikiewicz, *J. Mass Spectrom.* **2009**, *44*, 278–84.

[68] E. P. L. Hunter, S. G. Lias, *J. Phys. Chem. Ref. Data* **1998**, *27*, 413–656.
[69] R. G. Pearson, *J. Chem. Educ.* **1987**, *64*, 561.
[70] R. G. Pearson, *Inorg. Chem.* **1988**, *27*, 734–740.
[71] M. T. Rodgers, P. B. Armentrout, *Chem. Rev.* **2016**, *116*, 5642–5687.
[72] Y.-P. Ho, Y.-C. Yang, S. J. Klippenstein, R. C. Dunbar, *J. Phys. Chem. A* **1997**, *101*, 3338–3347.
[73] H. El Aribi, C. F. Rodriquez, T. Shoeib, Y. Ling, A. C. Hopkinson, K. W. M. Siu, *J. Phys. Chem. A* **2002**, *106*, 8798–8805.
[74] J.-D. Chai, M. Head-Gordon, *Phys. Chem. Chem. Phys.* **2008**, *10*, 6615.
[75] D. Corinti, B. Gregori, L. Guidoni, D. Scuderi, T. B. McMahon, B. Chiavarino, S. Fornarini, M. E. Crestoni, *Phys. Chem. Chem. Phys.* **2018**, *20*, 4429–4441.
[76] S. Osburn, V. Ryzhov, *Anal. Chem.* **2013**, *85*, 769–778.
[77] G. Bouchoux, J. Salpin, D. Leblanc, *Int. J. Mass Spectrom. Ion Processes* **1996**, *153*, 37–48.
[78] L. M. Bass, R. D. Cates, M. F. Jarrold, N. Kirchner, M. T. Bowers, *J. Am. Chem. Soc.* **1983**, *105*, 7024–7033.
[79] E. Hanozin, B. Mignolet, J. Martens, G. Berden, D. Sluysmans, A. S. Duwez, J. F. Stoddart, G. Eppe, J. Oomens, E. De Pauw, D. Morsa, *Angew. Chem. Int. Ed.* **2021**, *60*, 10049–10055.
[80] D. Corinti, A. Maccelli, M. E. Crestoni, S. Cesa, D. Quaglio, B. Botta, C. Ingallina, L. Mannina, A. Tintaru, B. Chiavarino, S. Fornarini, *Int. J. Mass Spectrom.* **2019**, *444*, 116179.
[81] J. C. Molano-Arevalo, W. Gonzalez, K. Jeanne Dit Fouque, J. Miksovska, P. Maitre, F. Fernandez-Lima, *Phys. Chem. Chem. Phys.* **2018**, *20*, 7043–7052.

Manuscript received: January 29, 2022
Accepted manuscript online: April 12, 2022
Version of record online: May 5, 2022